CFD analysis of coolant mixing in VVER-1000/V320 reactor pressure vessel

M. Böttcher [a], O. Bernard [b], A. Mas [b], V. Sanchez [a], R. Nop [c], F. Belaunde [c], C. Bourcier [d], D. Ruban [e], A. Hashymov [e], O. Halim [f,*], A. Pucciarelli [f], N. Forgione [f]

[a] Karlsruhe Institute of Technology (KIT), Institute for Neutron Physics and Reactor Technology, 76021 Karlsruhe, Germany
[b] FRAMATOME, 2 rue du professeur Jean Bernard, 69007 Lyon, France
[c] Université Paris-Saclay, CEA, Service de Thermo-hydraulique et de Mécanique des Fluides, 91191 Gif-sur-Yvette, France
[d] Université Paris-Saclay, CEA, Service de Génie Logiciel pour la Simulation, 91190 Gif-sur-Yvette, France
[e] ENERGORISK Ltd., 141, No7, Simyi Steshenkiv str., Kiev, Ukraine
[f] Università di Pisa, Dipartimento di Ingegneria Civile e Industriale, Largo Lucio Lazzarino 2, 56126 Pisa, Italy

ARTICLE INFO

ABSTRACT

This study presents a code-to-code and model-to-model comparison of coolant mixing in the VVER-1000/V320 Kozloduy Unit 6 nuclear power plant using Computational Fluid Dynamics (CFD). Four different CFD codes were used to simulate coolant mixing in the reactor vessel, namely ANSYS Fluent, ANSYS CFX, TrioCFD, and STAR-CCM+. Two different approaches were used to model the upper plenum, while a single simplified model was used for the reactor pressure vessel. The simulations were performed for VVER-1000 coolant transient benchmark (V1000CT-2) mixing exercise. The results were compared between the different CFD codes and models to assess the accuracy and consistency of the simulations with the available experimental data. Overall, the results showed good agreement between the different CFD codes and models, with minor differences observed in some cases. The simplified models were found to be sufficient for predicting the overall coolant mixing patterns observed in the reactor vessel, provided additional insights into the local flow structures and mixing characteristics. This study demonstrates the applicability and reliability of CFD simulations for coolant mixing analysis in VVER-1000/V320 nuclear power plants.

1. Introduction

The factors that influence the safe operation of Pressurized Water Reactors (PWRs) are numerous and complex. Thanks to decades of experience, Nuclear Power Plants (NPP) are designed according to established design criteria that consider reference accidents such as Main Steam Line Break (MSLB). MSLB is a design basis accident characterized by asymmetric cooling of the core accompanied by positive reactivity feedback. For such conditions of strong heterogeneities of flow and power distributions that occur in the core, it is necessary to quantify the mixing of coolant taking place in the reactor vessel during that accident. This may be important for several reasons, such as ensuring proper cooling for fuel rods and preventing overheating in the affected sector of the core. In-vessel mixing can be affected by various factors, such as the geometry of the vessel, the flow rate of coolant, the presence of spacer grids, etc. Understanding in-vessel mixing is thus essential for assessing the safety of nuclear reactors, ensuring design margins with respect to the Minimum Departure from Nucleate Boiling Ratio

(MDNBR) safety limit, and designing emergency response strategies in case of accidents.

Coupled 3D Neutron-Kinetics (NK) and 1D System Thermal-Hydraulics (STH) codes are often used in the state-of-the-art calculation chains for safety assessments of nuclear power plants. These codes are used to simulate the behaviour of the reactor core and coolant system under a wide spectrum of operating conditions and accident scenarios. Coupled 3D-NK and 1D-STH simulation allows for exchanging the feedback between the neutronics and thermal-hydraulics to be included in the simulation, which is important for accurately predicting the behaviour of the reactor under heterogeneous conditions. Nevertheless, the propagation of such heterogeneous fields of power and/or coolant through the downcomer and the lower plenum may not be accurately predicted by the mixing models implemented in 1D system codes and thus requires a support from experimental data and CFD analysis.

This issue is indeed discussed in the available literature. Ivanov et al. (2002) performed a safety analysis using coupled neutronic/thermal-hydraulic calculations and pointed out that the mixing occurring in

---

Nomenclature

CFD	Computational Fluid Dynamics
CAMIVVER	Codes And Methods Improvements for VVER comprehensive safety assessment
FA	Fuel Assembly
MDNBR	Minimum Departure from Nucleate Boiling Ratio
MSLB	Main Steam Line Break
NK	Neutron-Kinetics
NPP	Nuclear Power Plant
PWR	Pressurized Water Reactor
STH	System Thermal-Hydraulics
SG	Steam Generator
SIV	Steam Isolation Valve
VVER	Water-Water Energetic Reactor

the VVER-1000 vessel is regarded as an unresolved issue in the analysis of complex plant transients with reactivity feedback (Ivanov et al., 2002). Also, Espinoza et al. (2006), investigated the capability of the coupled approach and concluded that multi-dimensional thermal-hydraulic models are needed for a more realistic description of the coolant mixing phenomena within the VVER-1000 reactor pressure vessel (Espinoza et al., 2006). Another attempt by Kolev et al. (2008) studied the mixing matrix of VVER-1000 using CATHARE-2 and found that, while on one hand the integral parameters show a good agreement with the plant data, on the other the in-vessel mixing was reproduced in good qualitative agreement with the plant data; the temperature of large sector of the affected zone in the core was underestimated by approximately 4 K (Kolev et al., 2008).

Several studies were conducted to investigate in-depth the mixing in a Reactor Pressure Vessel (RPV) using CFD models. Bieder et al. (2007) used a coarse grid Large Eddy Simulations (LES) approach to study asymmetric flow distribution in a VVER-1000 reactor: the simulated domain starts at the RPV inlet nozzles up to the core support plate. The study concluded that CFD calculations correctly reproduced the core outlet temperature distribution and the measured rotation of the flow (Bieder et al., 2007). In addition, Höhne (2009), studied the VVER-1000 coolant mixing and performed a comparison of three CFD turbulence models: the flow domain included the inlets nozzles, downcomer, lower plenum, and a part of the core. The study showed that turbulence models could achieve consistent results when compared to the measured values: in particular, the rotation of the flow coming from Loop-1 was partly reproduced (Höhne, 2009). Later, Böttcher and Krüßmann (2010), used ANSYS CFX to fully model the VVER-1000 RPV, and extended the model to include a simplified primary loop namely the loop model. The authors modelled the hexagonal fuel assembly region as a subtracted circular part from its centre in order to reduce the grid cell counts. The study showed a good agreement between the plant data and the simulation for both of the models in terms of assembly outlet temperature distributions (Böttcher and Krüßmann, 2010). Recently, Cheng et al. (2016), carried out a CFD simulation using ANSYS FLUENT to model a four-loop VVER-1000 facing asymmetric operation conditions. The considered domain represented the full RPV with the adoption of porous media to model the core region. The study showed a good agreement with the integral parameters of the plant, demonstrating the capabilities and the potential of the use of "porous" approach (Cheng et al., 2016). Later, Feng and Bieder (2016) carried out a CFD simulation using TrioCFD. The Phenomena Identification and Ranking Table (PIRT) was adopted to build a full scale RPV model of VVER-1000 adopting the porous media approach to the core region. In this case, the authors showed that the flow rotation

calculated by the model at the core inlet underestimated the plant data and the maximum temperature was slightly overestimated (Feng and Bieder, 2016).

Lately, Spasov et al. (2021) have used the approach of multi-1D thermal-hydraulic models with RELAP/SCDAPSIM to study the vessel mixing phenomena in a VVER-1000. In their study, the authors developed two calculation models with different detail of vessel discretization and cross-flow: a 12-azimuth sector vessel model without radial discretization and a 24-sector model with radial discretization. The study concluded that both models predicted integral parameters in a generally good manner with respect to the reference plant data. Nevertheless, both models slightly underestimated the flow rotation occurring in the vessel. These issues suggested the need for further mesh refinement studies (Spasov et al., 2021).

As reported above, the larger number of the studies conducted on the in-vessel mixing of VVER-1000 slightly overestimating or only partially managed to reproduce the mixing occurring in the vessel. It is thus important to study thoroughly the in-vessel mixing of the VVER-1000 to guarantee the safe operation of the plant. CFD simulations can provide more accurate predictions of mixing in the RPV than the coupled 3D-NK and 1D-TH codes owing to their capabilities in taking into account the complex three-dimensional flow patterns and temperature distributions within the RPV. Nevertheless, a multiscale analysis approach could be deemed more valuable to study the vessel mixing phenomena in a VVER-1000, further details on the multiscale analysis approach can be found in the work performed by Bestion and Guelfi (2005) (Bestion and Guelfi, 2005). In fact, a mixing matrix could be generated from the CFD simulation which could be later used to support the system thermal-hydraulics codes in safety assessment: this would relevantly reduce the computational costs while allowing for suitable modelling of the reactor vessel mixing.

The problem of achieving suitable predictions of the mixing occurring inside a VVER reactor vessel is being addressed in the framework of CAMIVVER (Codes And Methods Improvements for VVER comprehensive safety assessment) project. A full-scale three-dimensional CAD model was developed aiming for an improved description of the coolant mixing phenomena within the VVER-1000 RPV using different commercial codes. The standard design of the VVER-1000/V320 is considered; the reference plant data are derived from the operational data of the Kozloduy Unit 6 nuclear power plant (NPP) provided in the technical report (Antoaneta et al., 1000). A simplified full-scale model based on the porous media approach is adopted and the V1000CT-2 thermal-hydraulics benchmark (Kolev et al., 2004) is chosen to validate the CFD models. With respect to the work conducted in the V1000CT-2 thermal-hydraulics benchmark, the present work may be regarded as an advancement for several reasons. Firstly, the modelled domain is not only limited to the vessel and core region but also extended to include the upper plenum section and the outlet nozzles. Secondly, the porous media approach is extended to model other regions and components such as the shielding tube block and several perforated sections in the VVER-1000. Finally, the larger computational power made available allows the use of finer computational grids and advanced meshing techniques, taking advantage of improved near-wall treatment such as the inflation boundary layers.

The present work is the result of the cooperation between several research institutions participating in the CAMIVVER project (CEA, ENERGORISK, FRAMATOME, KIT, and UNIPI). The primary aim of this research is to support and strengthen the use of CFD modelling in addressing mixing phenomena in the VVER-1000 reactor pressure vessel and investigating the applicability of simplified models of the entire reactor pressure vessel domain, including the implementation of a porous media approach. In the following, the results provided by each partner are reported: code-to-code comparisons are performed, and the

considered assumptions are discussed. A comparison with the available experimental data is performed as well.

2. Kozloduy-6 VVER-1000 steam generator isolation benchmark

The steam generator isolation experiment at Kozloduy Unit 6 was conducted as a part of a series of experiment designed for the commissioning of the NPP. The scope of this experiments was to investigate and examine the capability of vessel thermal-hydraulic models, as well as to quantify the in-vessel mixing. The main objectives of this benchmark were to quantify the following characteristics:

a) The mixing coefficients between each pair of loops, from cold legs to the inlet of fuel assemblies.
b) The azimuthal rotation (shift) of the loop flows with respect to cold leg axes.

2.1. Test case description "Reference benchmark exercise"

The benchmark test case can be divided into three phases: the initial phase, a transient phase, and a stabilized final phase. The initial phase started from a symmetric condition, where all the four main coolant pumps and four steam generators are in operation. The reactor was operated at a power of 281 MW, which is approximately 9.36 % of the

nominal operating conditions. The inlet coolant temperature of the reactor was 541.8 K which is about 20 degrees lower than the nominal value. Then, the transient phase is triggered by the closure of a steam isolation valve (SIV) which thus isolated steam generator (SG) no. 1 from feed water. Consequently, the pressure in the SG was first increased, then stabilized by controlled dumping of the steam into the condenser. As a result, the coolant temperatures in Loop-1 raised by 13.6 degrees and the mass flow rate decreased by approximately 3.6 %. The temperature in the other loops increased slightly due to the mixing of loop flows. Eventually, the final steady-state phase was reached 35 min after the isolation of the SG, resulting in a non-uniform core outlet temperature distribution. An azimuthal shift of the main loop flows with respect to the cold leg axes was observed as well.

It is important to mention that the parameters for the plant commissioning experiment were chosen in such a way that the reactivity feedback effects were kept to a minimum, and the thermal-hydraulics could be effectively isolated from the neutron kinetics. As a result, various conditions were established to minimize the impact of different feedback arising from boron acid concentration, coolant temperature reactivity, and the automatic power controller, all aimed at ensuring the separability between thermal-hydraulics and neutron kinetics. In addition, the reactor was operated at 9.36 % of the full nominal power to reduce the feedback of reactivity and improve the safety during the benchmark exercise. In this manner a nearly constant power distribution in the analysis of coolant transients was achieved and the reactor power
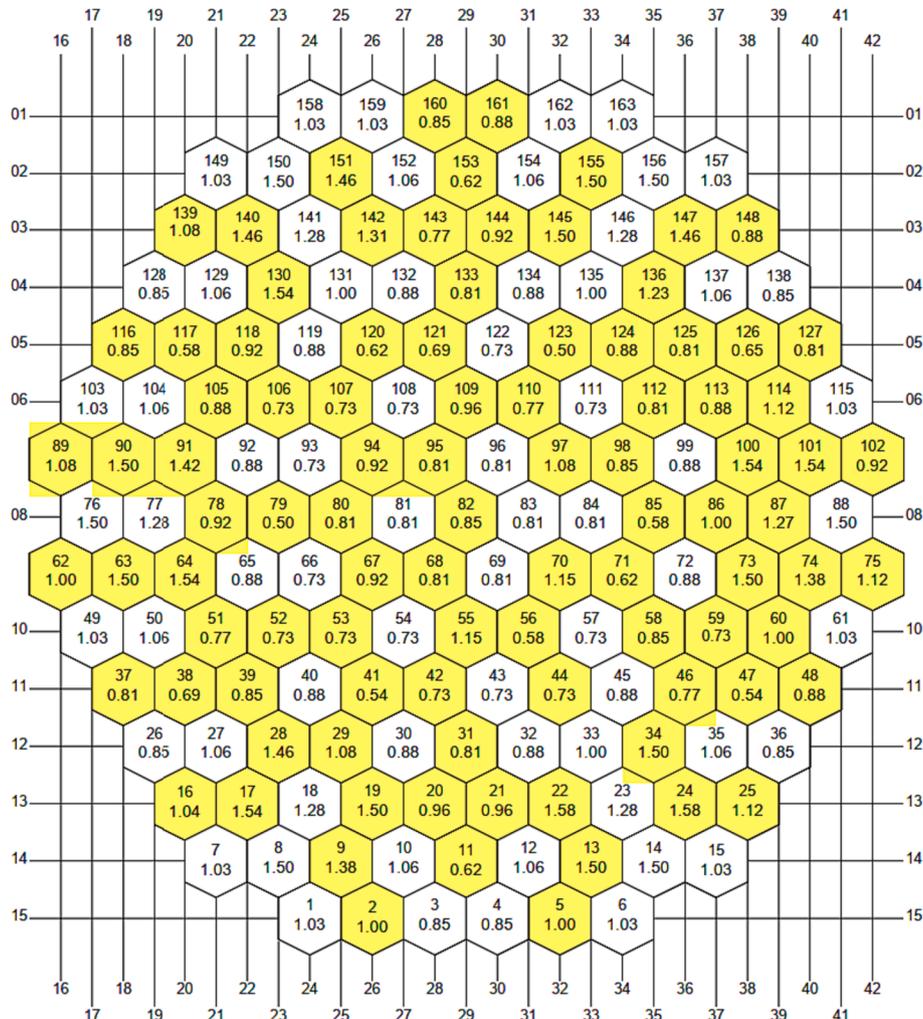
Fig. 1. Relative temperature rise in the fuel assemblies in the initial state: yellow – measured data, no color – estimated values. adapted from (Kolev et al., 2004)

changed by 0.16 % during the transient (Kolev et al., 2004).

Fig. 1 shows the measured and estimated relative temperature rise distribution in the initial state. Further details and specifications about the VVER-1000 coolant transient benchmark (V1000CT-2) can be found in (Kolev et al., 2004). It is worth noting that not all the Fuel Assemblies (FA) are instrumented by thermocouples: the temperature of instrumented ones only is reported in the core maps shown in Fig. 1. From this distribution, the FA inlet temperatures can be inferred assuming that the relative temperature rise distribution does not change during the transient, as follows,

$$T_{in,k} = T_{out,k} - dT_k(rel)*dT_{av(k)}; k = 1, \cdots, 163 \qquad (1)$$

$$dT_k(rel) = \frac{dT_k}{dT_{av(k)}}; dT_{av(k)} = \overline{\sum_k dT_k} \qquad (2)$$

where, $dT_k(rel)$ is the relative temperature rise distribution occurring during the initial steady-state.

2.2. Modelled domain

The VVER-1000/V320 is a pressurized water reactor with a thermal output of 3000 MW. The primary circuit of VVER-1000/V320 plants consists of four primary loops with horizontal SGs. The main design characteristics of VVER-1000/V-320 and the general layout of the reactor coolant system (based on Kozloduy Unit 6 data) are provided in Table 1 and Figs. 2 and 3. Further details and plant diagrams of the considered VVER-1000/V-320 reactor coolant system can be found in (Antoaneta et al., 1000).

The modelled flow domain includes the inlet nozzles, the downcomer, the elliptical bottom plate, the FA support columns, the core, the core basket, the shielding tube block, the barrel and the outlet nozzles. Fig. 4 shows the simplified flow domain model for the RPV developed in the frame of this work and adopted by FRAMATOME, CEA and UNIPI.

The main problem for the creation of a detailed CFD model for a geometrically highly complex technical system like the VVER1000 nuclear pressure vessel is to develop an adequate computational mesh that is able to resolve all relevant flow scales inside the pressure vessel while allowing for a suitable cell count. Though the vessel height is about 10 m and a diameter larger than 3 m, the smallest geometrical relevant scales are 3 mm wide, such as the gap width of perforations in the upper part of the core support columns. Consequently, and for practical reasons, in order to reduce the total cell count, several regions of the pressure vessel are meshed as porous media: the core, the upper part of the core support columns and nearly the complete part of the upper plenum.

Fig. 5 shows the model and mesh design adopted by KIT. The pipe parts entering and leaving the vessel were neglected because of their low influence on the mixing process inside the vessel. For computational grid

Table 1
General plant data from Kozloduy VVER-1000 / V320 Unit 6 (Antoaneta et al., 1000).

Item	Value	Dimensions
Coolant operating temperature – outlet	592.05	[K]
Average Coolant temperature	576.15	[K]
Coolant operating temperature – inlet	560.15	[K]
Reactor coolant flow	17,611	[kg/s]
Core exit pressure	15.75	[MPa]
Total volume of the vessel	110	[m³]
Total volume of the downcomer	18	[m³]
Total volume of the lower plenum	16	[m³]
Total volume of the upper plenum	61.2	[m³]
Coolant volume in the active core region	14.8	[m³]
Inlet nozzle ID	850	[mm]
Outlet nozzle ID	850	[mm]
Distance between hot and cold leg	1800	[mm]
Height of active fuel region (hot state)	3550	[mm]
Inner diameter of reactor pressure vessel	4136	[mm]

generation, a hybrid meshing technic is used. While the core region is discretized by a fully structured mesh, most of the other parts are modelled by tetra and prism elements (see inflated boundaries) with length scales adjusted to the expected flow structures. Especially for the downcomer and lower plenum boundary layer inflation technic was used. The limitation of meshing is clearly given by the (in general over proportional) increase of computational time with the number of cells, mainly for transient scenarios.

Fig. 6 shows the CAD model of the internal structures that are located inside the RPV as adopted by ENERGORISK. The elements of the lower plenum are simplified, such as the fuel assembly guide tubes modelled as straight tubes. Also, in the upper plenum, the perforated sections of the shielding drum as well as the upper section of the core barrel are modelled as porous regions. It is also worth to mention that the ENERGORISK CAD model fully resolves the internal structures of the upper plenum such as the shielding and control rods tubes as shown in Fig. 6.

2.3. Numerical models and boundary conditions

In the CAMIVVER Project WP6, one of the main focuses of the performed work is the validation of different CFD tools and models against the same coolant mixing data and the imposed boundary conditions. Results for V1000CT-2 mixing exercise have been submitted by 5 organisations from 4 countries. The main objectives of the considered coolant mixing test are the following:

- Evaluate the mixing coefficients i.e., (percentage of coolant provided by each cold leg to the inlet of fuel assemblies);
- Investigate the azimuthal shift (rotation) of loop flows from cold legs to the core inlet;
- Provide accurate data about the evolution of cold and hot leg temperatures during the transient phase of the test for comparison with the measurements;
- Identify the modelling issues with the highest impact on the CFD simulation's results.

In the following Table 2, an overview of the models and parameters used by the different participants for their CFD simulations is given: a more detailed model description for each partner can be found in the CFD models description report (Olivier et al., 2022).

Table 3 shows the integral parameters for the initial state before closing the SIV, the associated uncertainties to the integral parameters and the boundary conditions adopted by the different organizations. It is worth to mention that the total core flow rate assumed by UNIPI is 1 % smaller than the one considered by the other participants, as the model by UNIPI does not take into account the cold-hot leg bypass and thus the total mass flow rate decreased by the amount of flow that is expected to bypass the core through the spacer ring. Furthermore, it is worth noting that the CEA model used an imposed inlet velocity map accounting for swirl effects generated by the pumps. Considering this, the integrated mass flow at the inlet faces resulted in slight underestimation of the targeted plant flow rate, which nevertheless falls within the measurement uncertainties.

The heat source distribution in the reactor core is modelled in detail in accordance with the accurate descriptions of the power distribution of each FA provided for the VVER-1000 coolant transient benchmark (V1000CT-2). Fig. 7 presents the radial and axial power distribution maps used to impose the heat source in the core. In this work, the heat radial/axial power distributions represent a boundary condition: the considered values are in accordance with the addressed experimental measurements (Bestion and Guelfi, 2005). No coupled calculations are thus performed involving neutronics and a pure thermal-hydraulic was thus addressed.

In a porous media approach, the internal solid structures' volume is not exactly modelled; instead, it is substituted with the same volume of solid material isotropically distributed within the flow domain. It is
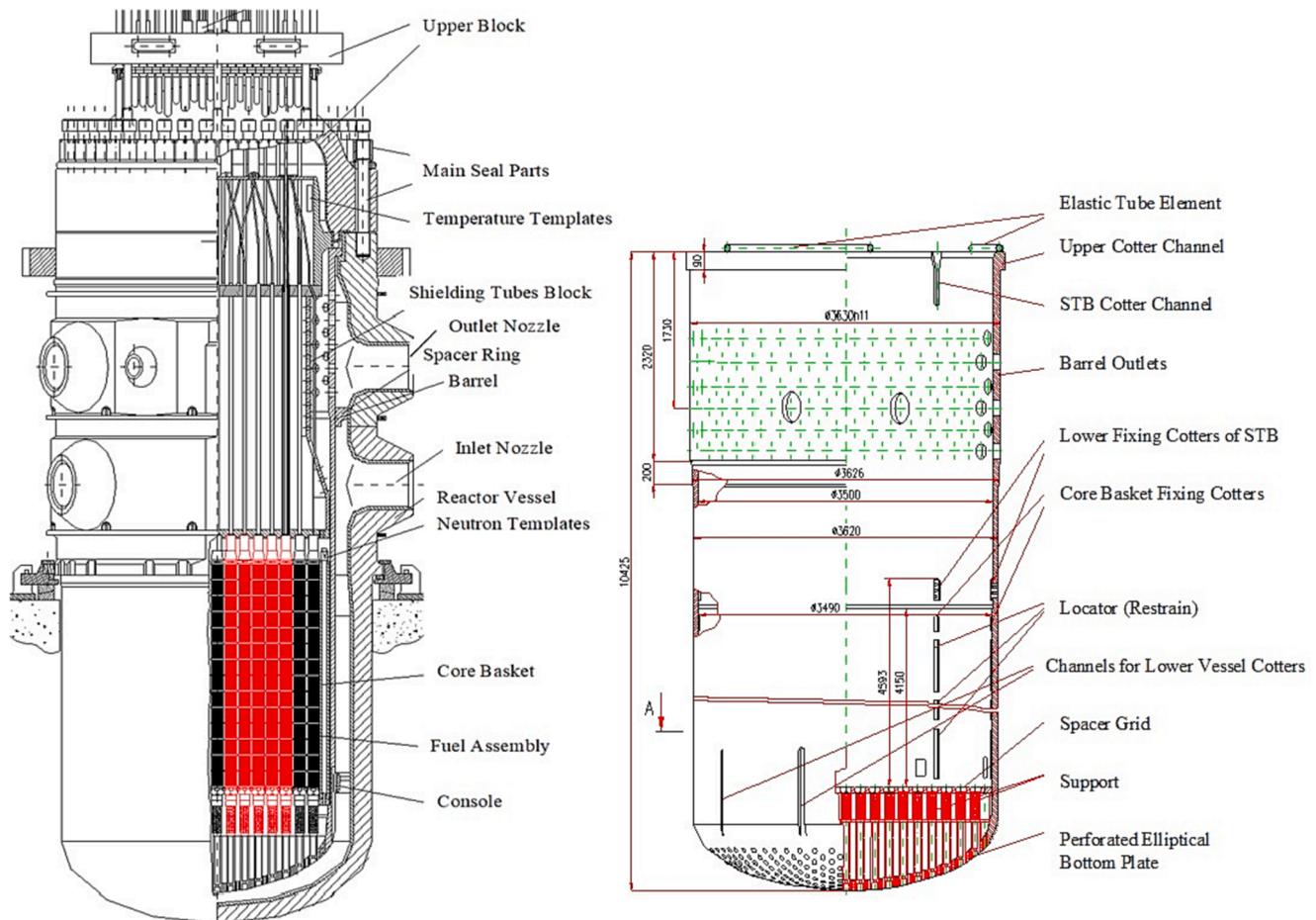
Fig. 2. Cross-sectional view of Reactor Pressure Vessel with reactor internals (left), Core barrel (right).
adapted from (Kolev et al., 2004)

worth noting that the porosity settings were established by evaluating the ratio of the internal structures' volume to the overall region's volume. Nevertheless, each participant made their distinct approximations and geometric simplifications. Table 4 provides an overview of the core porosity values utilized by the different participants.

The pressure loss in the porous media approach was addressed by introducing a momentum source term into the momentum equation. This source term comprises two components, a viscous loss term and an inertial loss term. The values of the porous resistances established through the calibration of loss coefficients, with the aim of reproducing the desired plant pressure drop at specified reference locations when the plant operated at full nominal power. Later on, the calibrated porous resistances were subsequently retained for the transient benchmark simulation. It is worth noting that each participant applied their own approximations at the basis of the adopted turbulence model and their respective simulation tools.

3. Results and discussion

In the present work, three types of results are collected and analysed: integral parameters, two-dimensional field distributions and temporal profile data. The collected results aim to validate the ability of CFD models to reproduce the targeted phenomena against the plant available data and to provide a detailed quantitative and statistical comparison for the selected target parameters. The analysis can be divided into two main categories: (a) Data-vs-prediction comparison and (b) Code-to-code comparisons highlighting the deviations for different codes and considered models.

3.1. Experimental data-vs-numerical predictions

Several parameters were selected for the assessment and validation of the results against the plant data: the pressure drop at some reference plant locations during the initial steady-state, the temporal profile of temperature at RPV loops outlets during the transient, the coolant temperature at fuel assembly outlets, loops coolant mixing coefficients and the azimuthal shift (rotation).

Table 5 reports the comparison between the measured and calculated values for the pressure drops at some relevant locations inside the reactor pressure vessel. It is important to note that the plant data refer to the initial state before closing SIV-1.

All the codes/models were able to provide an acceptable value for the overall reactor pressure losses with maximum deviation of about 10 % and in the core regions with maximum deviation of about 4 %. The best pressure drops predictions for the core are obtained by the UNIPI and ENERGORISK models. On the other hand, considering the total reactor pressure drop, the closest prediction to the plant data was provided by UNIPI. As it is important to highlight that the pressure drop in the core was achieved through a tuning process regarding the inertial resistance of the porous media considered for the very same regions.

The comparison between the temperature evolution predicted by the different participants for each of the four hot legs of the plant is shown in Figs. 8 to 11.

All models/codes were able to simulate the transient with deviations based on the model setup and the used tool. Concerning hot leg-1 the temperature increase within the first two seconds is predicted by all participants very well. Focusing on the whole transient, instead, both
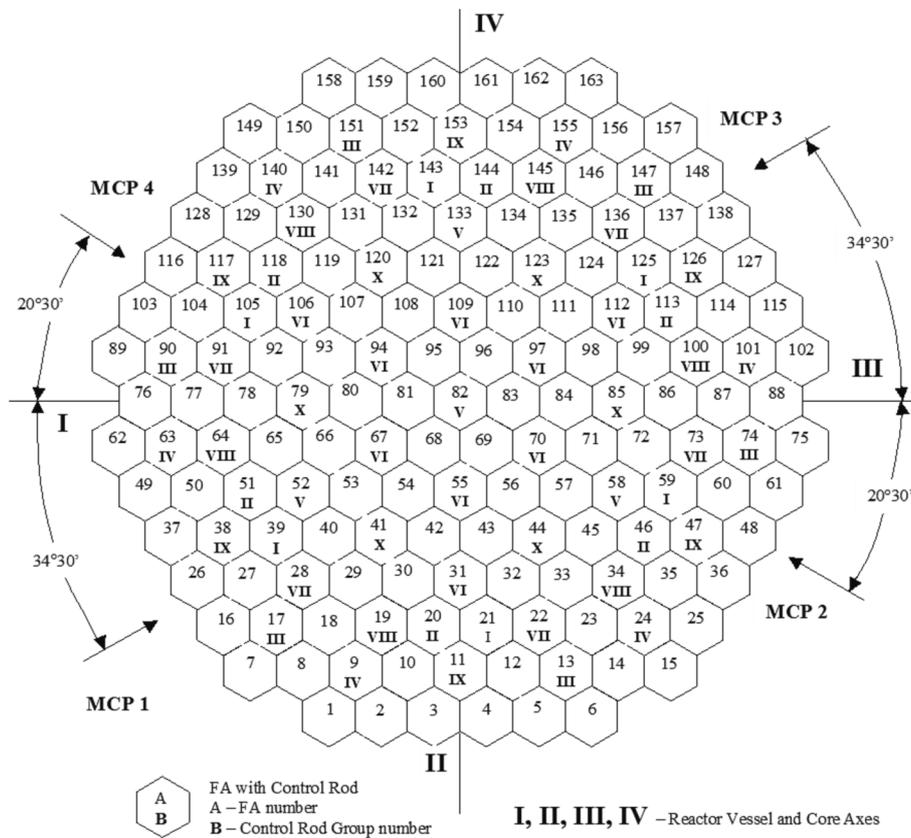
Fig. 3. Arrangement of fuel assemblies and inlets.
adapted from (Kolev et al., 2004)
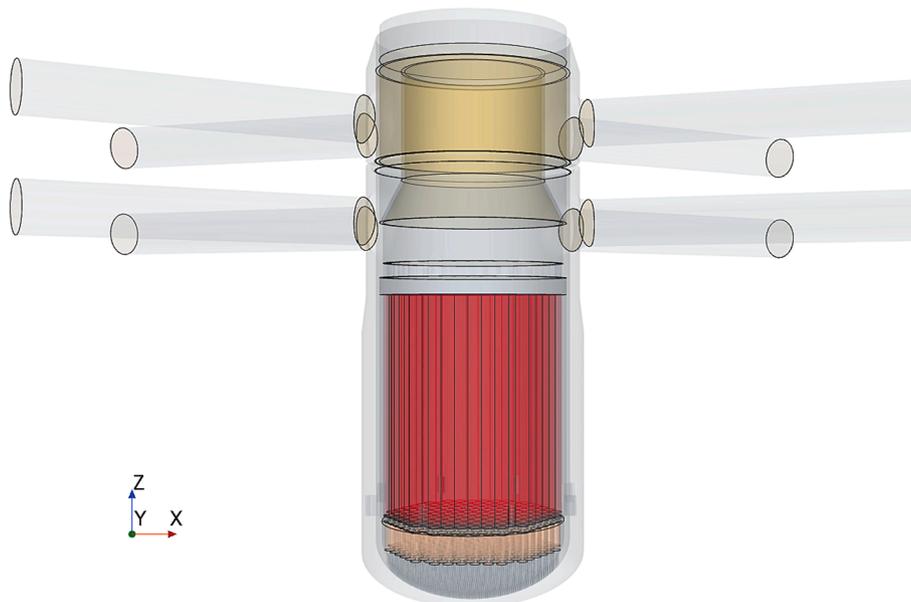
Fig. 4. VVER-1000 modelled for flow domain.

KIT and CEA (results available only for the first 600 s) reproduce the plant data very well; the models by UNIPI, FRAMATOME and ENER-GORISK are instead overestimating the final state temperature of about 2 K. Nevertheless, it must be highlighted that 2 K is indeed the uncertainty for temperature measurements in the addressed benchmark, all the provided results are thus included in the experimental data uncertainty range. It is worth mention that the CEA model has adopted a smoothed time-dependent interpolation of the cold leg-1 as a boundary condition: this explains their smoother hot leg-1 temperature predicted trend.

Moving to hot leg-2, all participants overestimated the observed moderate temperature increase reported by the experimental data. This is probably due to the fact that the amount of hot coolant coming from Loop-1 that enters into Loop-2 is too large. While the models by
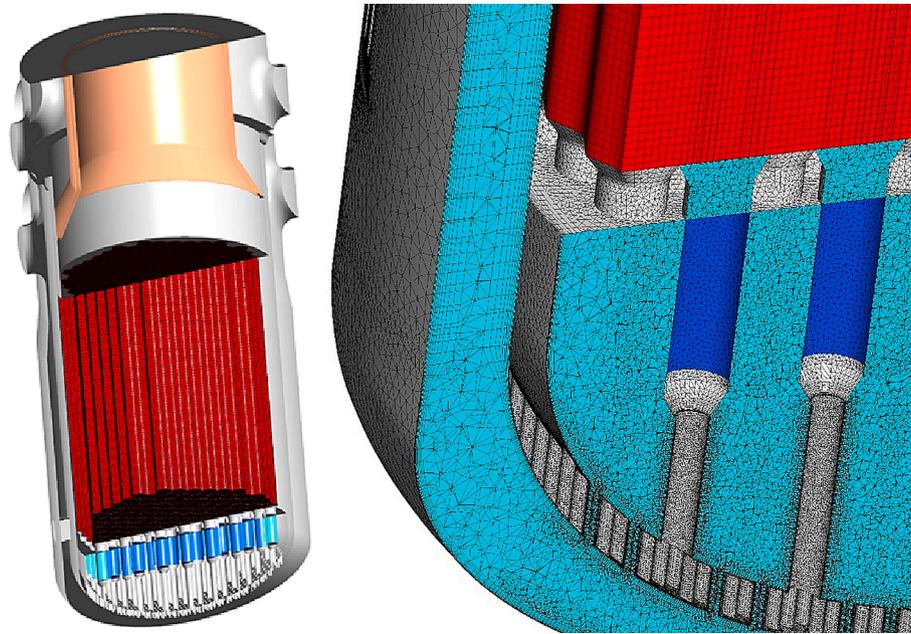
Fig. 5. The model by KIT with meshing detail in the lower plenum.
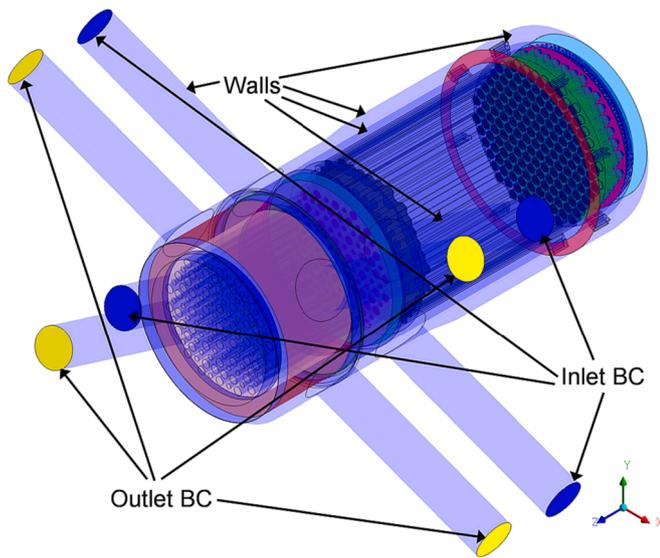
Fig. 6. RPV model by ENERGORISK and structures of the lower and upper plena.

FRAMATOME, UNIPI and ENERGORISK are over-predicting the temperature rise of about 1 K, thus inside the uncertainty range, the models by CEA and KIT are overestimating the final state temperature by nearly 4 K. For the KIT model, the reasons may be connected to the neglected diffusion in the upper plenum structures, a rather fine mesh in this region and to the added swirl at the inlets. CEA and KIT used additional pump swirl at the cold leg inlets which was adjusted mainly by the study of mixing in Loop-1. The rationale for the CEA model shows similar over-predicting as KIT model: it can mainly be attributed to the implementation of the pump swirl at the inlets, which needs to be adjusted in future studies by examining such phenomena in each individual loop.

Another reason for the over-prediction may be the instrumentation of temperature sensors, where each hot leg is equipped by 3 sensors located at various circumferential positions at the pipe walls. At an inner pipe diameter of 850 mm the sensors are not able to detect hotter temperatures at inner regions as calculated by the CFD models. As consequence, cross section averaged temperatures by CFD may be higher than measurement data.

In Loop-3, the model by CEA faced some issues since it was not able to predict the initial low frequency oscillations of the plant data. On the other hand, it must be stated that all the predictions are very close to the experimental data, well inside the experimental uncertainty range. Similar conclusions may be drawn also from the analysis of Loop-4. KIT and CEA provided predictions almost superimposed to the plant data, the other participants instead slightly overestimated the experimental results of about 0.5 K yet providing a very good prediction. It is worth to mention that the CEA model adopted a constant temperature values for cold legs 2, 3 and 4 as a boundary condition, which can be an important factor for justifying the flat temperature profiles at hot legs 2, 3 and 4, and not being able to capture the low frequency oscillations of the plant data.

Figs. 12 and 13 show the comparison between the experimental data and the prediction of the various participants for the coolant temperature distributions at the FA-outlet at initial (t = 0 s) and final (t = 1800 s) steady-states.

The analysis of the initial steady-state temperature distribution at the core outlet reports a systematic overestimation of roughly 0.5 K of the predictions provided by all participants with respect to the experimental data. This fact was also observed in a previous benchmark of the OECD in 2010 (Kolev et al., 2010). Nevertheless, according to the experimental data accuracy, values inside a ± 2 K range from the experimental measurements are to be considered to be in reasonable agreement with them. All the participants thus managed to provide a suitable prediction.

From the qualitative point of view, a good agreement is achieved as well at the final state. Nevertheless, it must be highlighted that larger discrepancies, locally up to 4 K are reported. This is probably due to the errors in the prediction of the coolant mixing inside the core. In fact, since the cold leg of Loop-1 provides a hotter fluid with respect to the others over the course of the transient, in the range of 10 K, wrong distributions of the flow inside the core may now lead to the observed temperature discrepancies. At the initial steady state, instead, since all the cold legs supply the coolant at the same temperature, this problem

Table 2
Overview of model and parameters used by the different CFD codes.

Organization	CEA	ENERGORISK	FRAMATOME	KIT	UNIPI
Country	France	Ukraine	France	Germany	Italy
Tool	TrioCFD	ANSYS Fluent	STARCCM+	ANSYS CFX	STARCCM+
Mesh type	unstructured	mainly structured	unstructured	unstructured	unstructured
Mesh elements	tetrahedral	hexahedral	polyhedral	mainly tetrahedral, hexahedral and prisms	polyhedral
Boundary layer inflation	no	linear narrowing of mesh layers (block topologies)	yes	yes (not everywhere)	yes (only used in fluid regions)
No of elements (millions)	32	15.4	48	36	27.6
Element size	6 mm – 130 mm	5 mm – 32 mm	8 mm – 80 mm	5 mm – 50 mm	20 mm – 100 mm
CAD model	FRAMATOME	FRAMATOME	FRAMATOME	FRAMATOME	FRAMATOME
Downcomer	Fluid domain	Fluid domain	Fluid domain	Fluid domain	Fluid domain
Core region	Porous media	Porous media	Porous media	Porous media	Porous media
Lower plenum	Fluid domain	Fluid domain	Fluid domain	Fluid domain	Fluid domain
Upper part of core support columns	Porous media	Porous media	Porous media	Porous media	Porous media
Upper plenum	Porous media	CAD extensions (shielding and control rods tubes are considered) - Fluid domain	Porous media	Porous media	Porous media
Turbulence model	Standard k-ε	k-ω (SST)	k-ε low Re	k-ω (SST)	Standard k-ε
Physical properties	T dependent at 15.6 MPa	T dependent at 15.6 MPa	T dependent At 15.6 MPa	IAPWS tables with p and T dependency	T dependent at 15.6 MPa
Spatial discretization	VEF (finite volume elements)	2nd order	2nd order	Higher order method Blending 1st −2nd ord.	2nd order
Time integration	1st order Implicit Euler	2nd order	2nd order	2nd order Euler back-ward	2nd order
Cold to hot leg bypass	Not modelled	Modelled	Not modelled Mass flow at the inlets as in the reference test	Not modelled Mass flow at the inlets reduced by 1 %	Not modelled Mass flow at the inlets reduced by 1 %
Core basket bypass	Not modelled	Modelled	Modelled	Modelled; mass flow rate ~ 3 %	Modelled; mass flow rate ~ 3 %
SWIRL	Consideration of additional pump swirl at the cold leg inlets	No	No	Consideration of additional pump swirl at the cold leg inlets	No

Table 3
Comparison of the boundary conditions at the initial state before closing the SIV.

Parameter	Data	Uncertainty	CEA	ENERGORISK	FRAMATOME	KIT	UNIPI
Core power [MW]	281	± 60	281	281	281	281	281
Cold leg-1, T [K]	541.72	± 1.5	541.75	541.72	541.72	541.72	541.72
Cold leg-2, T[K]	541.65	± 1.5	541.85	541.65	541.65	541.65	541.65
Cold leg-3, T [K]	541.88	± 1.5	541.75	541.88	541.88	541.88	541.88
Cold leg-4, T [K]	541.85	± 1.5	541.75	541.85	541.85	541.85	541.85
Hot leg-1, T [K]	545.0	± 2	544.36	544.64	544.79	544.64	544.81
Hot leg-2, T [K]	545.0	± 2	544.5	544.67	544.86	544.74	544.89
Hot leg-3, T [K]	544.9	± 2	544.65	544.74	544.91	544.75	544.92
Hot leg-4, T [K]	545.0	± 2	544.77	544.79	545.01	544.91	545.04
Cold leg-1, Q [kg/s]	4737	±110	4721	4737	4737	4737	4690
Cold leg-2, Q [kg/s]	4718	±110	4612	4718	4718	4718	4671
Cold leg-3, Q [kg/s]	4682	±110	4667	4682	4682	4682	4635
Cold leg-4, Q [kg/s]	4834	±110	4894	4834	4834	4834	4785
Core flow rate(inc. bypass) [kg/s]	18,971	±440	18,893	18,971	18,971	18,971	18,782

was not observed. For these reasons, the analysis of the mean absolute errors provided in Table 6 shows a significant increase in deviations between the initial and final state for all participants. The assembly number refers to the location of the maximum deviation from the plant data. Also, it is worth noting that at t = 1800 s despite the increase in deviations between the initial and final state, all models predicted the maximum deviation to be found in the second quarter of the core corresponding to Loop-2.

The comparison of the mixing coefficients predicted by the different participants with the experimental data is reported in Figs. 14 to 17. Each figure focuses on one of the RPV cold legs.

All the codes/models managed to provide a qualitatively reasonable trend for the mixing coefficients for all the four loops. However, it must be highlighted that some models provided better results than others; in addition, some models predicted large mixing coefficients in regions where the referred cold leg should not provide any contribution. For instance, all participants managed to predict the mixing coefficient values of cold leg-1 with some degree of deviation between the model and the plant data up to assembly no. 100. From assembly no. 100 to 163, instead, all the models, except for the one by FRAMATOME, show a decaying behaviour for the flow coming from cold leg-1 as observed in the experiments (see Fig. 14).

A similar conclusion can be drawn from the analysis of the mixing coefficients of the other cold legs: good predictions are usually reported
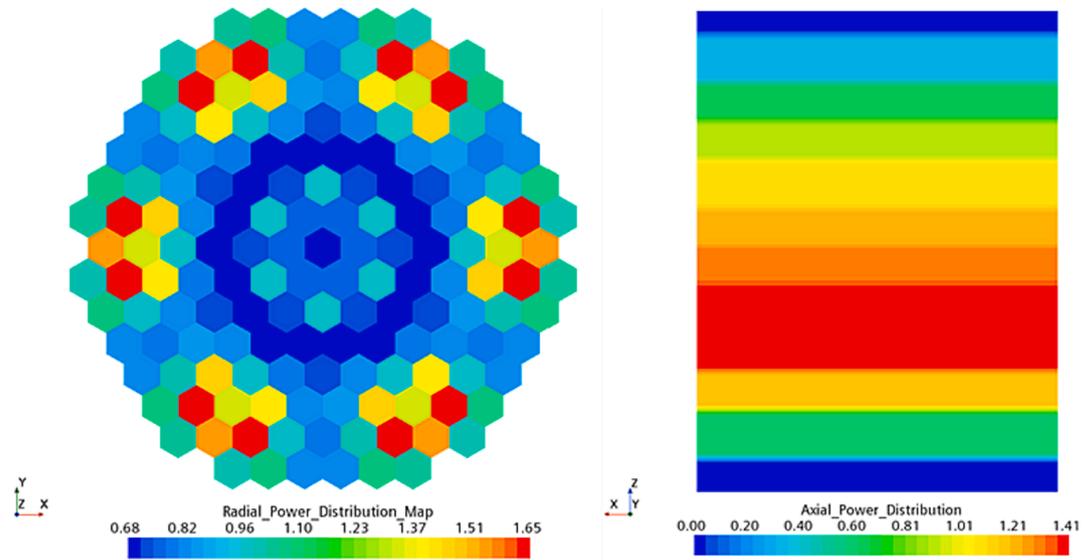
Fig. 7. Radial and Axial power distribution maps.

Table 4
Core porosity adopted by the different participants.

	CEA	ENERGORISK	FRAMATOME	KIT	UNIPI
Core porosity	0.54	0.5887	0.46	0.5385	0.55

Table 5
Comparison of the pressured drop predicted by the different participants with the reference data.

ΔP	ΔP data [MPa]	FRAMATOME	KIT	UNIPI	ENERGORISK
Reactor pressure drop	0.418	0.446	0.376	0.407	0.378
Core pressure drop	0.149	0.154	0.155	0.143	0.142
Upper plenum losses	0.042	0.058	0.031	0.038	0.036

for the core region mainly fed by the referred cold leg while larger deviations are reported for more mixed regions. Each partner overpredicts or underpredicts these regions depending on the adopted model and assumptions. Statistical analyses of the average absolute deviations for the different predictions with respect to the plant data are summarized in Table 7. The best predictions were provided by CEA, ENERGORISK which managed to often keep the error below 10 %; the other participants usually deviate more than 10 %, with UNIPI and FRAMATOME sometimes reaching 14 %.

The mixing coefficients were calculated only for the initial state case because of the lack of experimental data during the transient. Figs. 18 and 19 presents the distribution of the mixing coefficients for Loop-1 and Loop-2 against the local angular assembly positions at the core outlet. Furthermore, the central angular position of minimum coolant mixing in each loop for the plant data is shown (see indications "data centreline").

The purpose of this analysis is to determine the central position of the lowest coolant mixing for each loop in terms of the angular difference against the central cold leg inlet nozzle positions. In principle, this can be done by the analysis of passive tracer fields mixing coefficients for each loop or by analysis of temperature differences as for plant data, where the higher temperature at the inlet of cold leg-1 of about 10 K was
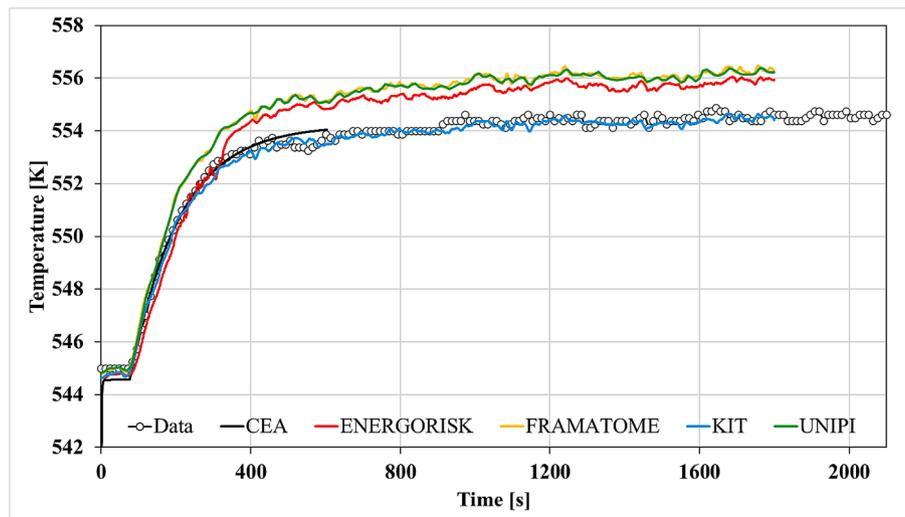
Fig. 8. Comparison between the hot leg-1 temperature predicted by the participants and the measured data for the considered transient scenario.
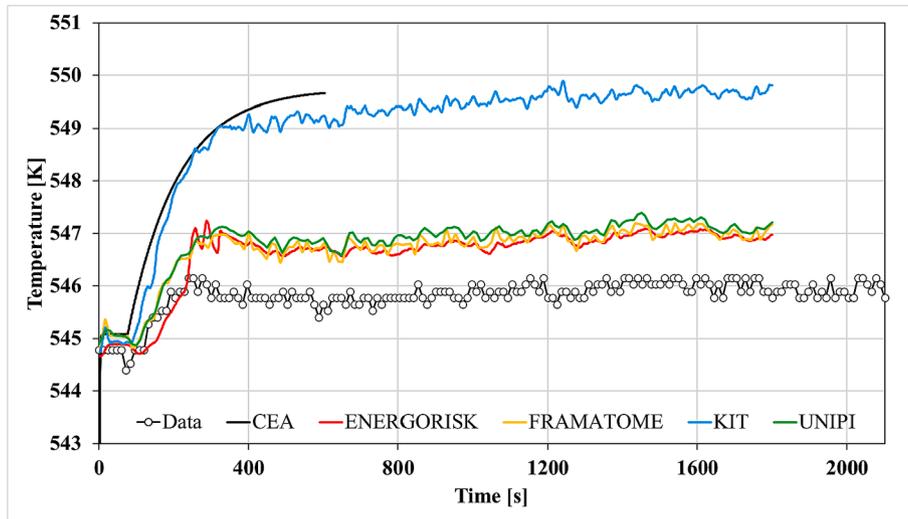
Fig. 9. Comparison between the hot leg-2 temperature predicted by the participants and the measured data for the considered transient scenario.
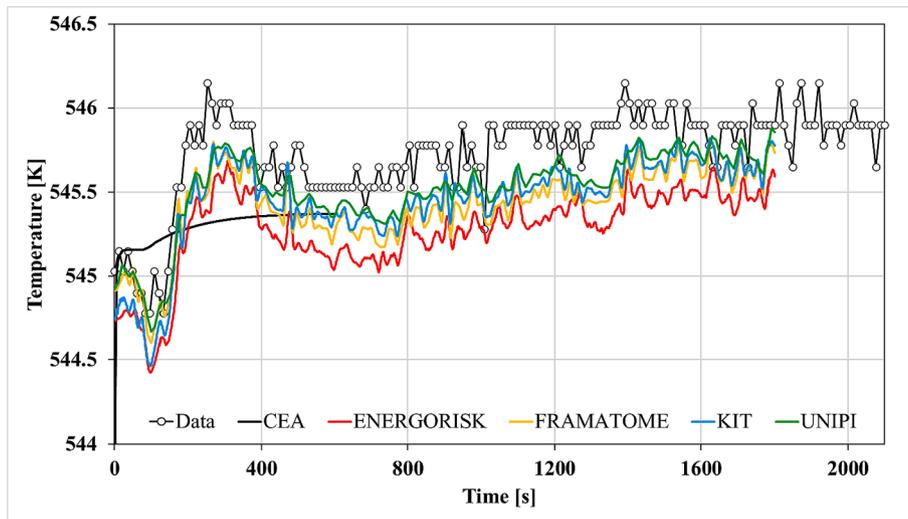
Fig. 10. Comparison between the hot leg-3 temperature predicted by the participants and the measured data for the considered transient scenario.
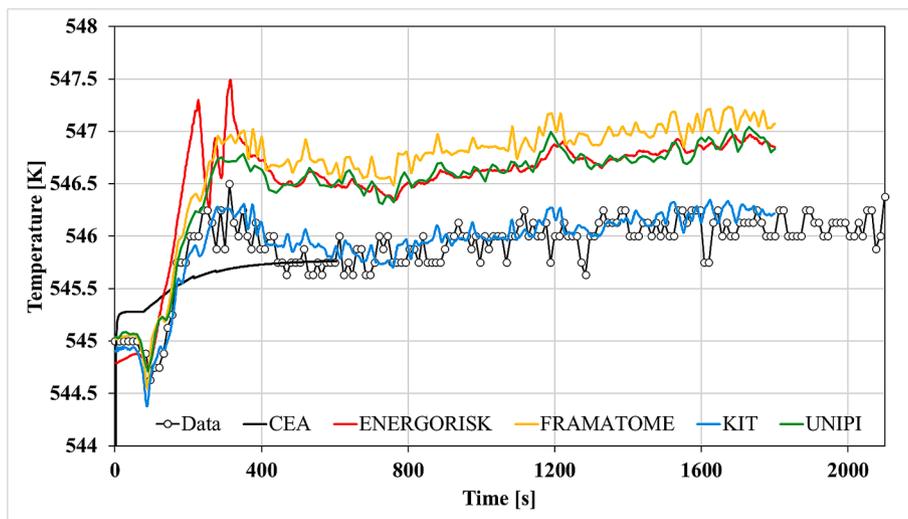
Fig. 11. Comparison between the hot leg-4 temperature predicted by the participants and the measured data for the considered transient scenario.
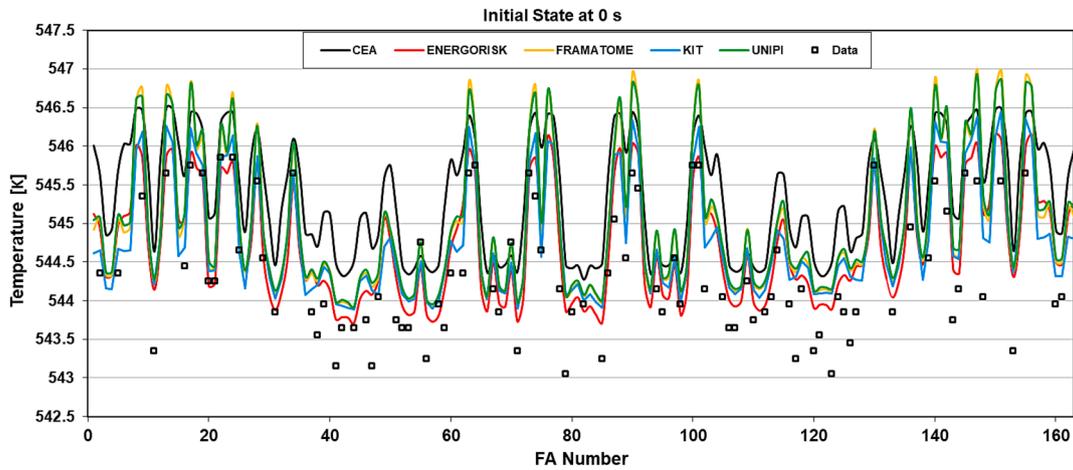
Fig. 12. Comparison between the experimental and numerical results for the coolant temperature distribution at the FA-outlets at 0 s.
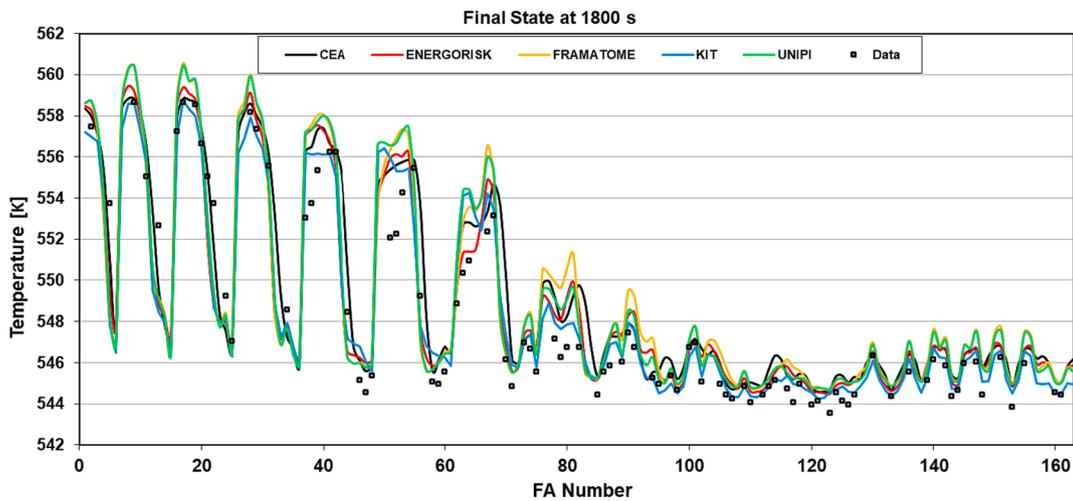
Fig. 13. Comparison between the experimental and numerical results for the coolant temperature distributions at the FA-outlets at 1800 s.

Table 6
Statistical error of the predictions for the FA outlet average temperature [K] versus plant data.

t = 0 s / 1800 s	CEA	ENERGORISK	FRAMATOME	KIT	UNIPI
av. deviation	0.93 / 1.10	0.39 / 1.14	0.66 / 1.50	0.46 / 0.92	0.68 / 1.38
max. deviation	1.82 / 4.25	1.07 / 4.80	1.50 / 5.71	1.06 / 5.94	1.54 / 5.47
Assembly no.	102 / 56	148 / 22	136 / 5	117 / 5	136 / 5

used as tracer (by neglecting the thermal diffusion).

The best agreements at the core outlet for Loop-1 were obtained by the CEA and KIT models. The reason could be related to the added swirl component at the cold leg inlets. The suggested swirl by KIT was adjusted mainly by obtaining the best agreement for this loop.

Table 8 presents the angular rotation with respect to the referred cold leg nozzle positions for all loops: measured and predicted results for the core outlet are here compared. Results at the core inlet based on temperature differences for Loop-1 are shown as well. Concerning Loop-1, the models show the lowest deviations, in the range of 2°, against plant data. Larger values, especially for Loop-4, were instead reported for the other loops. It has to be mentioned that the plant data are based on temperature differences: therefore Loop-1 data should have the relative best accuracy compared with the data of the other loops. The angular turns of the other loops are calculated with significant larger deviations between the models and the plant data. Unfortunately, no information about the experimental uncertainties is reported in the benchmark specification. The models with lowest deviations for all loops are the ones by CEA and KIT. Both models use additional pump swirl at the cold leg inlets compared with the other models. The overall tendency of the models is to underestimate the angular turn.

Between core inlet and core outlet the angular rotation of Loop-1 increases from 26.5° to 28.8°: this seems to be reasonable because the imposed swirl continues downstream, though at decreasing strength as a consequence of damping by friction due to core structures and dissipation in the fluid. At the core inlet a former OECD benchmark provided a value of 26° which is in reasonable agreement with the present analysis.

3.2. Code-to-code comparisons

For the code-to-code comparison, variables such as coolant temperature, coolant velocity at core inlet for both the initial and final states were selected. Figs. 20 and 21 present the coolant temperature
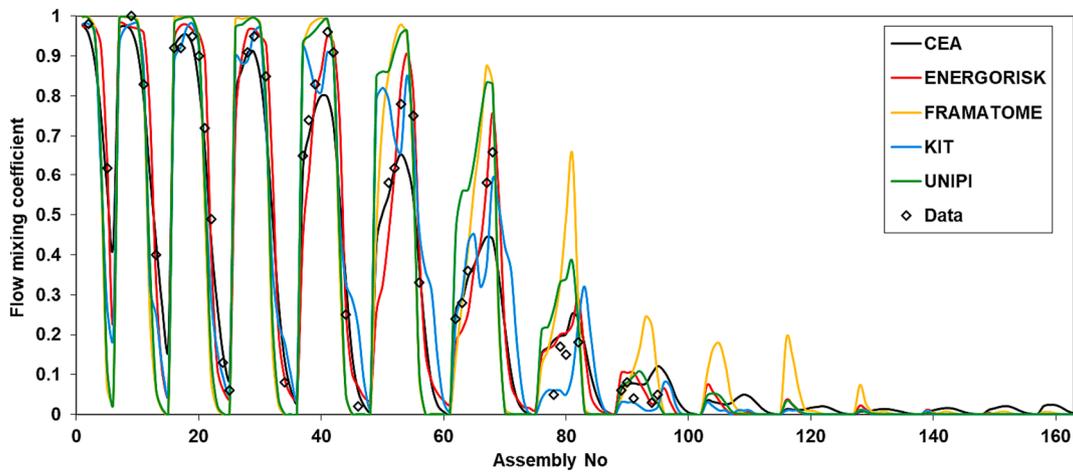
Fig. 14. Comparison of the measured and predicted coolant mixing coefficient for the cold leg of Loop-1.
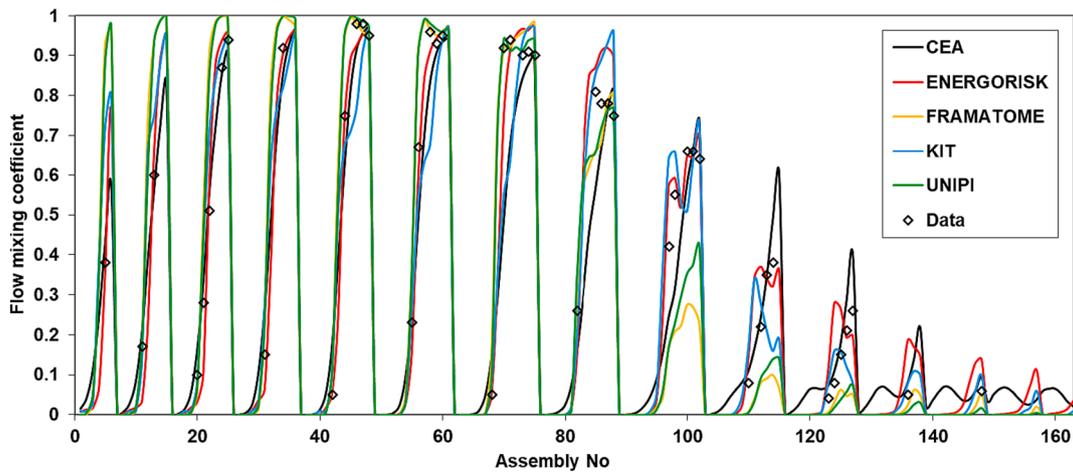
Fig. 15. Comparison of the measured and predicted coolant mixing coefficients for the cold leg of Loop-2.
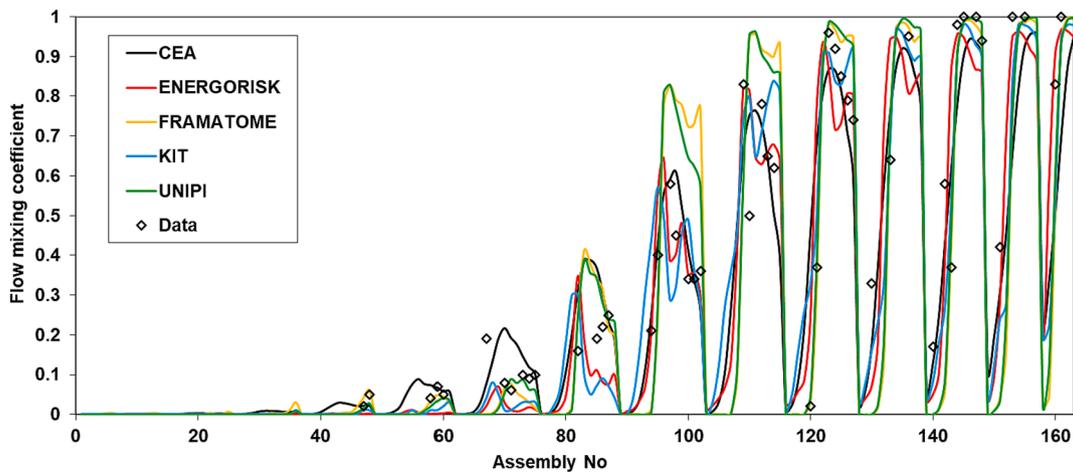
Fig. 16. Comparison of the measured and predicted coolant mixing coefficient for the cold leg of Loop-3.

distribution at the core inlet for the initial (t = 0 s) and final (t = 1800 s) steady-states. For the initial steady-state, all the model predictions agree sufficiently well for the core inlet temperature distributions; the deviation between the models is less than 1 K. For the final state, instead, all the considered models managed to achieve a good agreement with the plant data: the CEA model provides an overestimating trend for the plant

data. The discrepancies, even for the CEA prediction are usually inside the 2 K uncertainty range; success can thus be claimed.

Figs. 22 and 23 present the coolant velocity distribution at the core inlet for initial (t = 0 s) and final (t = 1800 s) steady-states. Both figures show that the maximum variation between all the models is only 3 m/s for some of the peaks.
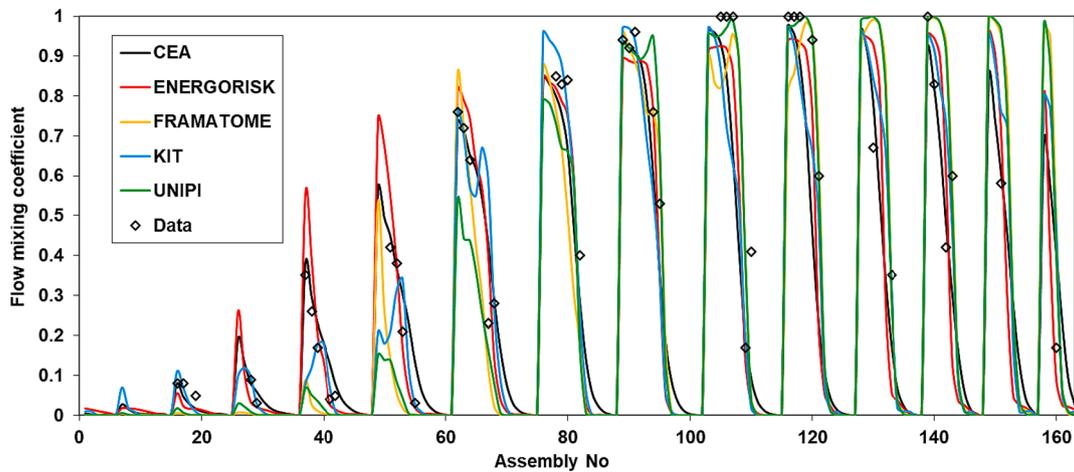
Fig. 17. Comparison of the measured and predicted coolant mixing coefficient for the cold leg of Loop-4.

Table 7
Average absolute deviation of model results vs. data and maximum deviation of model results.

	Loop-1	Loop-2	Loop-3	Loop-4	av. 1 ~ 4	Max. 1 ~ 4
CEA	0.060	0.081	0.111	0.099	0.088	0.48
ENERGORISK	0.082	0.071	0.114	0.108	0.094	0.49
FRAMATOME	0.135	0.134	0.148	0.145	0.141	0.55
KIT	0.079	0.109	0.116	0.118	0.106	0.39
UNIPI	0.150	0.121	0.135	0.139	0.136	0.50

Among the main causes of the discrepancies observed in Figs. 22 and 23 between the codes, the role of meshing and wall boundary resolution for the downcomer, the elliptical bottom plate, and of the porous media model for the core support columns must be mentioned. In addition, different concepts for the bypass modelling may provide significant uncertainty. Furthermore, different core porosity factors as shown in Table 4 are one of the reasons for the deviations observed between the models.

Between the core inlet and outlet, the flow undergoes a significant pressure loss of approximately 1.4 bar, which homogenizes the velocity and mass-flow profiles. Compared with old benchmark results (see Fig. 24), the differences between the several models have become smaller. For the final state at the core inlet, the range for velocities varies from 4.2 m/s to 8.2 m/s in the OECD benchmark and decreased to vary from 3.9 m/s to 6.9 m/s in the current study which demonstrates a slightly decrease of model uncertainty.

The decrease of the differences in the obtained predictions is probably due to the improved and bigger computer hardware (leading to larger models with smaller cell sizes and less numerical diffusion), improved meshing technics and more advanced porous media models.

In fact, the meshing tools adopted in this work (mainly purposely developed for the related CFD code) make boundary layer refinement possible also in highly complicated geometries and can generate smoother transition regions between anisotropic regions like walls and more isotropic regions. Furthermore, some commercial CFD tools like STARCCM + support polyhedral cell types that allow for a reduction of the cell numbers and therefore further lower the computational costs. Semi-automatic meshing techniques have reduced the development time of models significantly; nevertheless, it must be mentioned that meshing has still a large impact and it shows a high sensitivity to model results.

Concerning porous media modelling; improvements were achieved
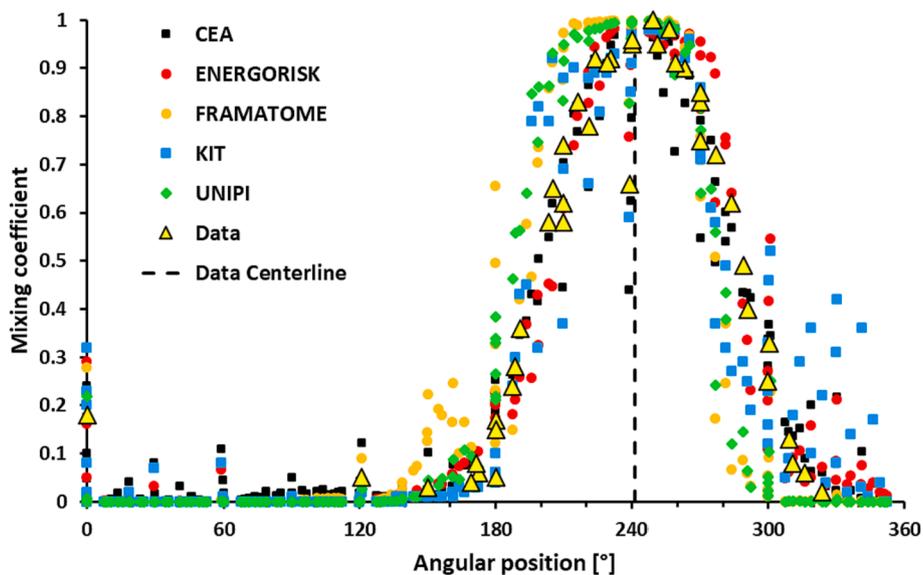
Fig. 18. Angular position of mixing coefficients for Loop-1.

13
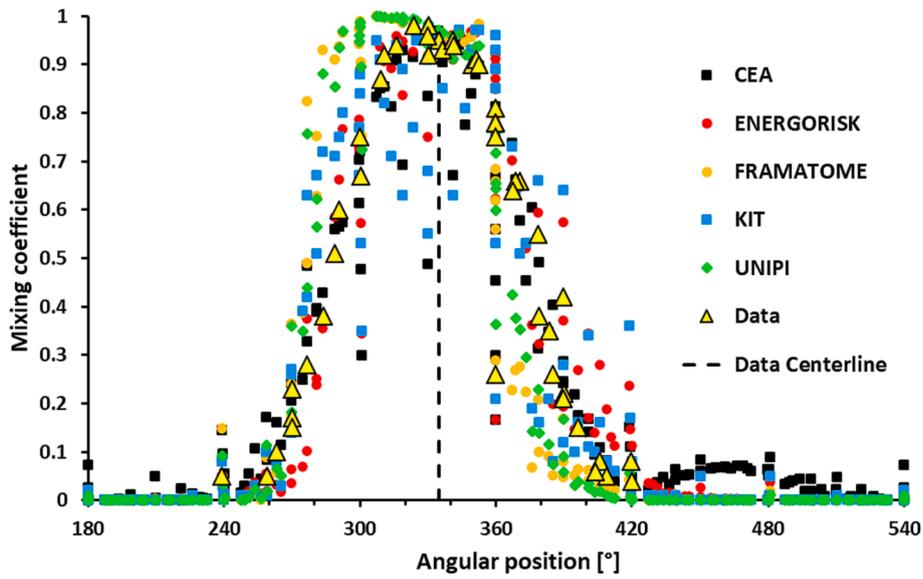
Fig. 19. Angular position of mixing coefficients for Loop-2.

Table 8
Angular turn analysis.

Ang. Turn [°]	Data	CEA	ENERGORISK	FRAMATOME	KIT	UNIPI	Average deviation against data
Loop-1[a]	28.8	27.1	34.0	22.8	28.0	21.2	−2.2
Loop-2[a]	−4.6	−6.8	−5.1	−20.2	−3.0	−3.0	−3.0
Loop-3[a]	30.8	23.7	41.3	17.0	26.6	26.6	−3.8
Loop-4[a]	−5.0	−3.3	−16.1	−25.5	−3.0	−19.0	−8.4
Loop-1[b]	26.5	26.6	22.9	24.8	30.7	25.5	−0.4

[a] core outlet, mixing coefficient analysis, initial state.
[b] core inlet, temperature difference analysis, final state.
CEA and KIT models are using pump swirl at cold leg inlets.
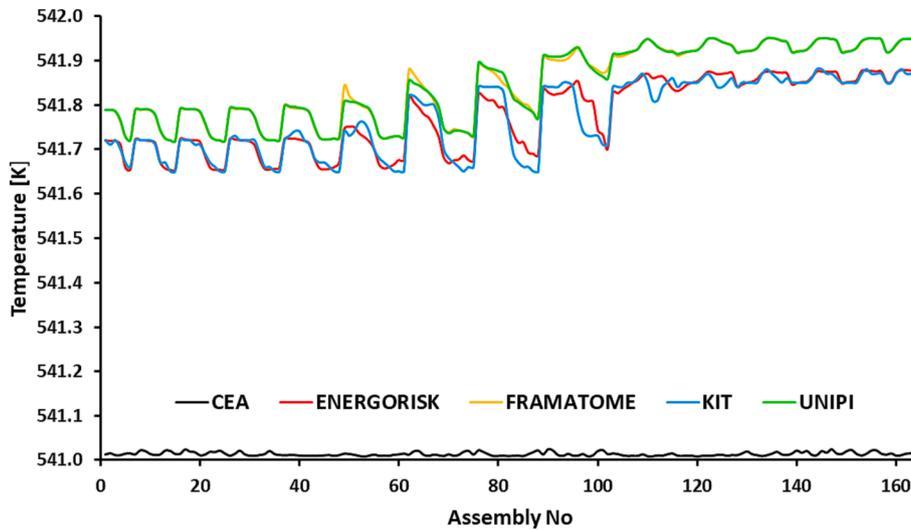
Fig. 20. Predicted coolant temperature distribution at the core inlet for the initial state 0 s.

for the implementation of anisotropic source terms for momentum and energy and a more sophisticated handling of the solid phase. Also, the numerical robustness of the solvers due to the handling of meshes with partially poor-quality cells has reduced the development time for highly complex CFD models.

4. Conclusions

The considered benchmark problem is comparable to a former benchmark led in 2010 by OECD. The results of the benchmarks can be directly compared because the simulated scenario is completely
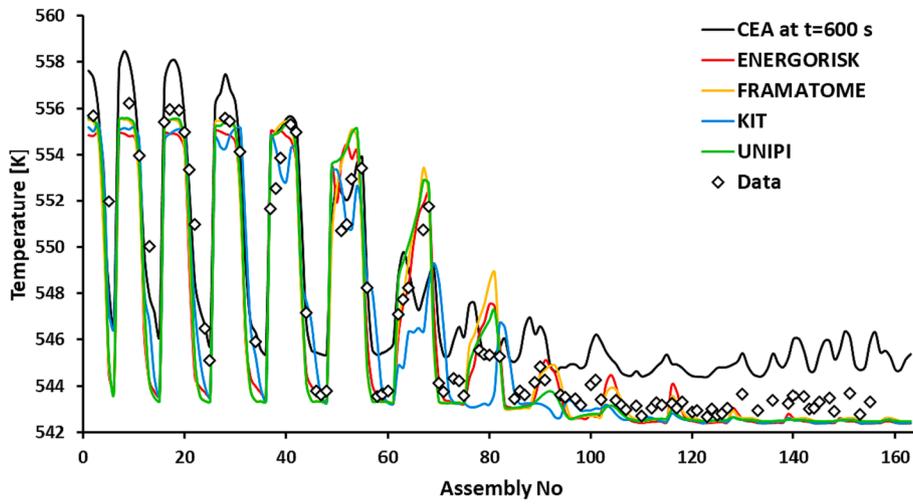
Fig. 21. Predicted and measured coolant temperature at the core inlet for the final state 1800 s.
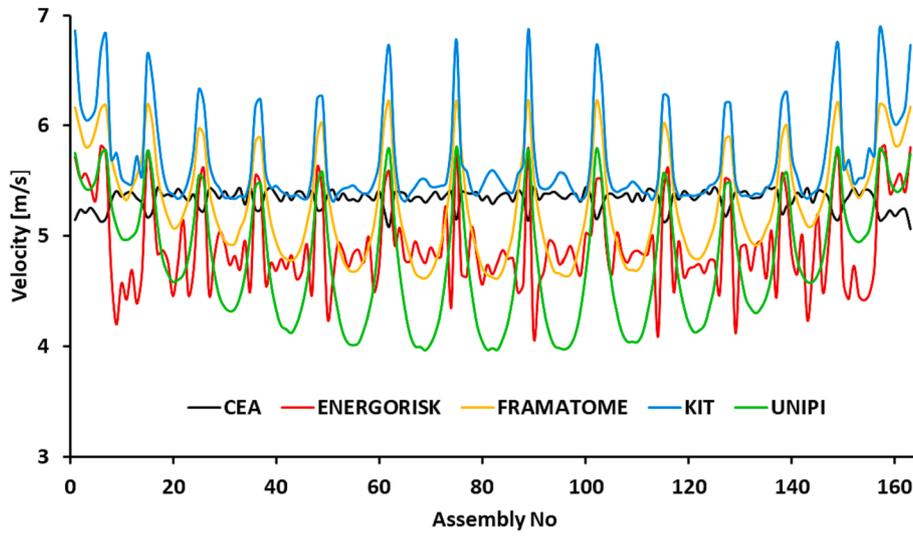
Fig. 22. Predicted coolant velocity at the core inlet for the initial state 0 s.
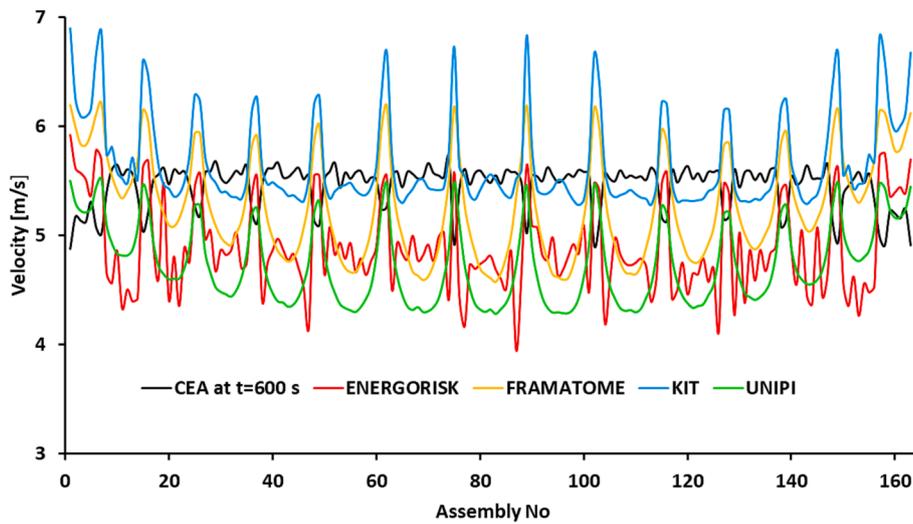
Fig. 23. Predicted coolant velocity at the core inlet for the final state 1800 s.
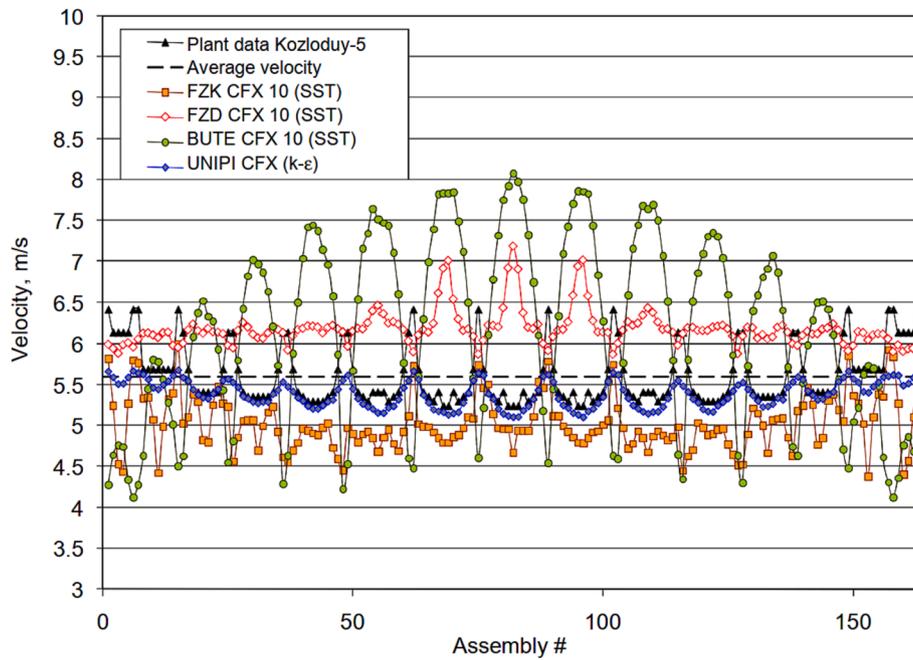
Fig. 24. Assembly-by-assembly core inlet velocities in the final state OECD benchmark results (2010) (Kolev et al., 2010).

identical. The present analysis concluded an overall quantitatively good agreement for plant data with some deviations between the participant models. Predictions of angular turn could be improved by the consideration of swirl at the cold leg inlets. As well as in the old benchmark, large deviations in the predictions of velocities at the core outlet could be observed but at a decreased level.

The improvements in the results of the new benchmark are a consequence of increased computer capabilities, improved physical models and solver technics in CFD software, such as the ones related to porous media approaches. Further advances were obtained by the implementation of additional swirl at the cold leg inlets. Eventually, significant improvements are to be related to the development of new meshing technics during the past decade.

In 2010, the average number of cells of the participant models was about 5.2 million and has increased to 27 million together with smaller time steps. Additionally, most participants were using a 1st order upwind scheme because of higher numerical stability and for the compensation of missing turbulent diffusion by additional numerical diffusion.

In the present benchmark, instead, the goal was modelling all structures in the flow path from the inlets to the core inlet by resolving details as much as possible while upper plenum structures are considered mainly by porous media models (such as the core and the upper part of core support columns). While on the one hand all participants had to limit the cell number in order to obtain reasonable computational times for the transient scenario, the simplifying assumptions allowed for achieving sufficiently reliable predictions of the considered data set.

From the analysis of deviations and the comparison with the older benchmark the conclusion can be drawn, that a mesh with a more spatial resolution of details but a coarser resolution of boundary layers is in advance towards a mesh with a finer resolution of wall boundaries but with additional porous media regions.

A possibility of further improvement may be the tuning of the mixing process in porous media regions like the core or core support columns (by fitted turbulent Prandtl and/or Schmidt numbers, sources for turbulent kinetic energy etc.) while pursuing for a spatial resolution of structures with impact on coolant mixing as far as possible.

CRediT authorship contribution statement

M. Böttcher: Investigation, Formal analysis, Writing – review & editing. **O. Bernard:** Investigation, Formal analysis, Writing – review & editing. **A. Mas:** Investigation, Formal analysis, Writing – review & editing. **V. Sanchez:** . **R. Nop:** Investigation, Formal analysis, Writing – review & editing. **F. Belaunde:** Investigation, Formal analysis, Writing – review & editing. **C. Bourcier:** Investigation, Formal analysis, Writing – review & editing. **D. Ruban:** Investigation, Formal analysis, Writing – review & editing. **A. Hashymov:** Investigation, Formal analysis, Writing – review & editing. **O. Halim:** Investigation, Formal analysis, Writing – review & editing. **A. Pucciarelli:** Investigation, Formal analysis, Writing – review & editing. **N. Forgione:** Investigation, Formal analysis, Writing – review & editing.

Declaration of Competing Interest

The authors declare that they have no known competing financial interests or personal relationships that could have appeared to influence the work reported in this paper.

Data availability

Data will be made available on request.

Acknowledgements

References

Antoaneta, Stefanova, Neli, Zaharieva, Petia, Vryashkova, Pavlin, Groudev. D3.2 - The CAMIVVER Definition report with specification for NPP with VVER 1000 reactor with respect to selected transients (2020).

Bestion, D., Guelfi, A., 2005. Multiscale analysis of nuclear reactors thermal-hydraulics-the Neptune project. La Houille Blanche 91 (5), 65–74.

Bieder, U., Fauchet, G., Bétin, S., Kolev, N., Popov, D., 2007. Simulation of mixing effects in a VVER-1000 reactor. Nucl. Eng. Des. 237 (15–17).

Böttcher, M., Krüßmann, R., 2010. Primary loop study of a VVER-1000 reactor with special focus on coolant mixing. Nucl. Eng. Des. 240 (9), 2244–2253.

Cheng, J.-P., Yan, L.-M., Li, F.-C., 2016. CFD simulation of a four-loop PWR at asymmetric operation conditions. Nucl. Eng. Des. 300, 591–600.

Espinoza, S., Hugo, V., Böttcher, M., 2006. Investigations of the VVER-1000 coolant transient benchmark phase 1 with the coupled system code RELAP5/PARCS. Prog. Nucl. Energy 48 (8).

Feng, Q., U. Bieder. 2016. CFD Analysis of a Steam Generator Separation Test in the Kozloduy VVER-1000 Reactor." In NUTHOS-11 The 11th International Topical Meeting on Nuclear Reactor Thermal Hydraulics, Operation and Safety.

Höhne, T., 2009. CFD Simula1tion of thermal-hydraulic benchmark V1000CT-2 using ANSYS CFX. Sci. Technol. Nucl. Install.

Ivanov, B., Ivanov, K., Groudev, P., Pavlova, M., Hadjiev, V., 2002. VVER-1000 coolant transient benchmark. Nea/nsc/doc 6.

Kolev, N., S. Aniel, E. Royer, U. Bieder, D. Popov, Ts Topalov. "VVER-1000 Coolant Transient Benchmark (V1000CT), Volume II: Specifications of the VVER-1000 Vessel Mixing Problems." Commissariat a l'Energie Atomique and OECD Nuclear Energy Agency (2004).

Kolev, N. P., E. Royer, and I. Spasov. VVER-1000 Coolant Transient Benchmark. Phase 2 (V1000CT-2), Summary Results of Exercise 1 on Vessel Mixing Simulation. Nuclear Energy Agency, Organisation for Economic Co-operation and Development, 2010.

Kolev, N.P., Sabotinov, L., Petrov, N., Nikonov, S., Donov, J., 2008. Validation cases of CATHARE 2 for VVER-1000 main steam line break analysis. J. Power Energy Syst. 2 (2).

Olivier, Bernard, Michael, Böttcher, Artur Hashymov, Denis, Ruban, Ulrich, Bieder, Raksmy, Nop, Ossama, Abedelhalim, Andrea, Pucciarelli. "D6.1 – Description of CFD models from partners Results of outlet flow distribution benchmark (2022).".

Spasov, I., Gerova, G., Filipov, K., Grigorov, A.l., Kolev, N.P., 2021. Simulation and integrated uncertainty analysis of the OECD/NEA V1000CT2 vessel mixing problem with RELAP/SCDAPSIM mod3. 5. In: AIP Conference Proceedings, 2333. AIP Publishing LLC, p. 090026.